Self-Assembly of Cricoid Proteins Induced by "Soft Nanoparticles": An Approach To Design Multienzyme-Cooperative Antioxidative Systems

Hongcheng Sun,[†] Lu Miao,[†] Jiaxi Li,[†] Shuang Fu,[†] Guo An,[†] Chengye Si,[†] Zeyuan Dong,[†] Quan Luo,[†] Shuangjiang Yu,[‡] Jiayun Xu,[†] and Junqiu Liu*[,†]

[†]State Key Laboratory of Supramolecular Structure and Materials, College of Chemistry, Jilin University, 2699 Qianjin Street, Changchun 130012, China and
[‡]Key Laboratory of Polymer Ecomaterials, Changchun Institute of Applied Chemistry, Chinese Academy of Sciences, 5625 Renmin Street, Changchun 130021, China

ABSTRACT A strategy to construct high-ordered protein nanowires by electrostatic assembly of cricoid proteins and "soft nanoparticles" was developed. Poly(amido amine) (PAMAM) dendrimers on high generation that have been shown to be near-globular macromolecules with all of the amino groups distributing throughout the surface were ideal electropositive "soft nanoparticles" to induce electrostatic assembly of electronegative cricoid proteins. Atomic force microscopy and transmission electron microscopy all showed that one "soft nanoparticle" (generation 5 PAMAM, PD5) could electrostatically interact with two cricoid proteins (stable protein one, SP1) in an opposite orientation to form sandwich structure, further leading to self-assembled protein nanowires. The designed nanostructures could act as versatile scaffolds to develop multienzyme-cooperative antioxidative systems. By means of inducing catalytic selenocysteine and manganese porphyrin to SP1 and PD5, respectively, we successfully designed antioxidative protein nanowires with both excellent glutathione peroxidase and superoxide dismutase activities. Also, the introduction of selenocysteine and manganese porphyrin did not affect the assembly morphologies. Moreover, this multienzyme-cooperative antioxidative system exhibited excellent biological effect and low cell cytotoxicity.

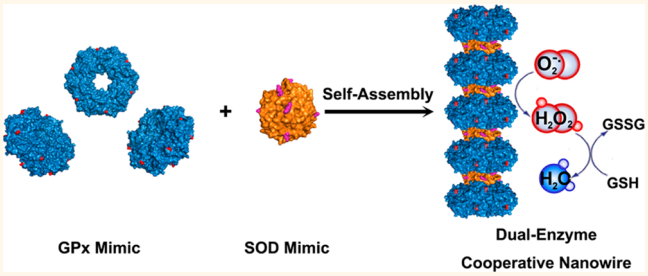

KEYWORDS: PAMAM dendrimer · cricoid protein · protein nanowire · multienzyme-cooperative · artificial selenoenzyme · antioxidation

As the most important biomacromolecules in living organisms, proteins are involved in almost all biological activities in molecular levels. Contemporary biomedical researchers and material scientists have focused their research interests on designing and fabricating protein assemblies with unique functions or structures, and are trying to apply them in high-performance biomimetic materials.[1−5] Over the past decades, the explosive research of supramolecular chemistry has promoted the innovative revolution of the protein assembly to enrich the assemble strategies and disclose the protein assembly behaviors in organisms.[6] Electrostatic interaction,[7] host−guest interaction,[8] metal-mediated interaction,[9] and other interactions[10,11] have been employed in fabricating the protein assemblies. Electrostatic self-assemblies are among the most powerful and effective approaches in constructing various hierarchical protein nanosuperstructures due to their surface inherent charge distributions.[12]

Stable protein one (SP1), isolated from aspen plants (*Populus tremula*), is a boiling stable, stress-responsive protein with no significant sequence homology to other stress-related proteins.[13−15] Six dimers bind together *via* hydrophobic interaction to create a homododecameric cricoid protein nanoring around a pseudo 6-fold axis (C_6 symmetry), with an outer and inner diameter of about 11 and 2.5 nm, respectively, and a height of 4.5 nm (Scheme 1a,c). Researchers have employed some positively charged "rigid nanoparticles" to

* Address correspondence to junqiuliu@jlu.edu.cn.

Received for review March 1, 2015 and accepted May 7, 2015.

Published online May 07, 2015
10.1021/acsnano.5b01311

© 2015 American Chemical Society

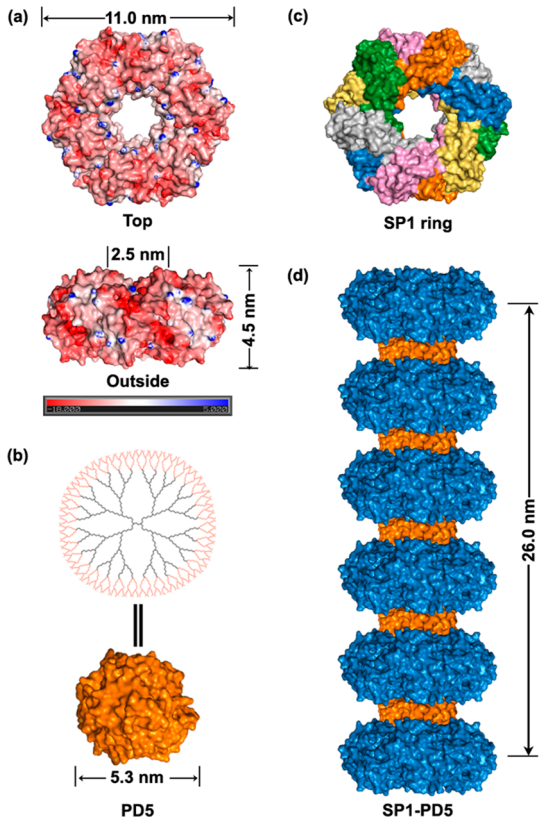

Scheme 1. Structure-based design of protein nanowires. (a) The top and outside view of SP1 surface charge distribution. The red and blue represent negative charges and positive charges, respectively. (b) The irregular globular structure (orange) represents the surface topography of generation 5 PAMAM dendrimer (PD5). (c) Overview of the SP1 homododecameric cricoid structure assembled by hydrophobic interaction. (d) Assembly model of one SP1 nanowire composed of six SP1 nanorings (blue) and five PD5 dendriemers (orange).

accurately control the protein self-assembly behavior and to guide the "growth" direction to form nanowires. Medalsy *et al.* developed SP1−GNP chains through the gold nanoparticles (GNP) medicated interaction with mutant 6His-SP1,[16] because the GNP could further serve as a linker to form protein−GNP chains once attached to the 6His-SP1.

For the wild-type SP1 protein, computer simulations show the acidic amino acid residues (negatively charged, red color) are enriched in the top and bottom surfaces of the cricoid structure, while the alkaline residues (positively charged, blue color) are mainly focused on its inside and outside surfaces (Scheme 1a). The heterogeneous charge distribution makes it possible for the positively charged nanoparticles to directionally combine with top or bottom surface to form regular protein nanoarrays. In our previous work, we have demonstrated that positively charged quantum dots (QDs) with diameter about 3−10 nm behaved as linkers to connect SP1 together to form nanowires through multielectrostatic interactions, so that the positive charges around the QDs could interact with the negative charges enriched in the top surface of SP1.[17]

These "rigid nanoparticles" can guide the "growth" of SP1 for their regular symmetrical morphologies and rigid nanostructures. The success of SP1 assembling to nanowires prompted us to investigate if "soft nanoparticles" could also guide the self-assembly of cricoid proteins. It is a great challenge for scientists to drive proteins with organic unimolecules, which may greatly enrich the protein assembly strategies. Since a single electrostatic interaction is too weak to operate, multiple electrostatic interactions on a nanoparticle are considered in this work to realize "multivalency" interactions with proteins. Dendrimer is a type of uniform distributed organic macromolecules with defined size, shape, and placement of functional groups. We can accurately control its size only by adjusting the dendrimer generations. Poly(amino amine) (PAMAM) dendrimers,[18−20] with a variety of amino groups distributed around the molecular surface, may be the most ideal "soft nanoparticles" to guide the cricoid proteins assembly. PAMAM is positively charged at physiological conditions, while SP1 is negatively charged (the isoelectric point (p*I*) is about 4.3).[13] The opposite charges distribution makes it possible to assemble into nanowires by electrostatic interaction as the QDs induced SP1 assembly behavior.

We further planned to utilize an electrostatic self-assembly method to build up functional protein nanowires. Creating artificial enzymes that mimic the complexity and help to understand the principle of natural systems hs been a great challenge over the past two decades.[21−23] Recently, our group reported a new glutathione peroxidase (GPx) mimic using SP1 as scaffold, and exhibited excellent GPx activity.[15] In fact, enzymes in organisms always act in a cooperative or a synergistic way to keep bodies in balance and healthy.[24] The normal metabolism of organism produces various kinds of reactive oxygen species (ROS) in the membranous or the aqueous compartments of the cells. GPx can only catalyze the reduction of hydroperoxides as well as H_2O_2, but for another main ROS in organism, superoxide radical anions ($O_2^{-\bullet}$) can only be scavenged by superoxide dismutase (SOD). Unfortunately, this method can only investigate the function of single enzyme, not the complexity of synergistic enzyme systems.

Inspired by our previous work, we developed a novel strategy to construct SP1 protein assembly triggered by electrostatic interaction of multicationic PAMAM dendrimers and SP1 rings. The PAMAM dendrimer in the molar ratio of 1:1 could induce SP1 protein rings into nanowires in aqueous solution. By means of inducing GPx and SOD centers to protein and PAMAM dendrimer, respectively, we designed a dual-enzyme-cooperative antioxidative nanowire with both GPx and SOD activities to *in vitro* mimic the synergistic enzyme catalytic process *in vivo*.

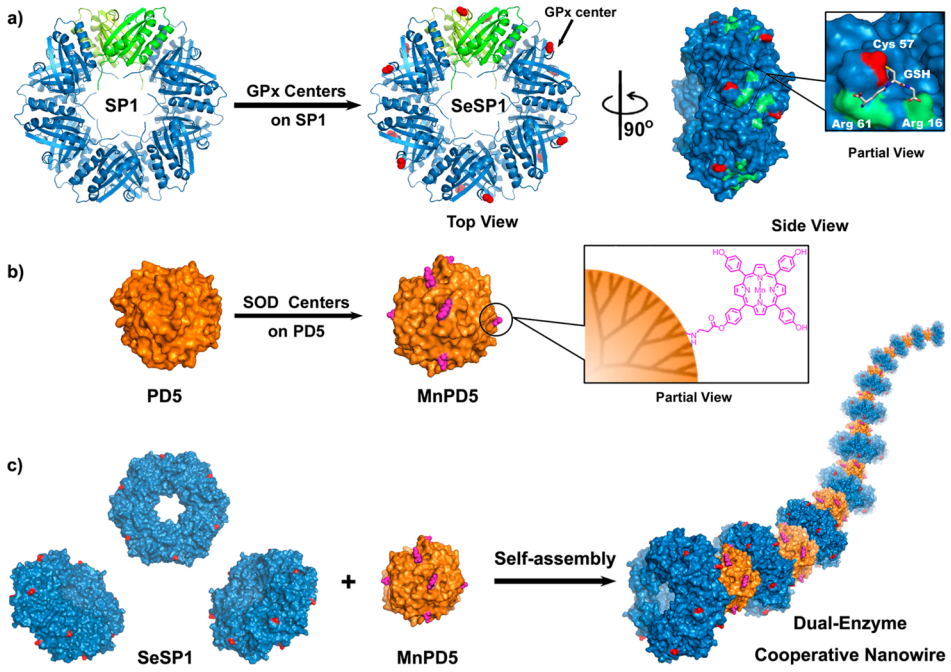

Scheme 2. Design of dual-enzyme cooperative antioxidative system with both GPx and SOD activities. (a) GPx catalytic center, selenocysteine (red), is designed on the outer surface of SP1. (b) SOD catalytic center, manganese porphyrin (magenta), is modified on the surface of PD5. (c) Assembly model of SeSP1−MnPD5 nanowire with SeSP1 (blue) and MnPD5 (orange).

RESULTS AND DISCUSSION

Construction of Catalytic Centers on SP1 and "Soft Nanoparticle". The "soft nanoparticle" should feature three key elements in guiding the SP1 growth direction to highly ordered nanowires: (1) The "soft nanoparticle" should interact with SP1 along its C_6 symmetry axis. (2) The "soft nanoparticle" must be large enough to ensure that two SP1 rings can be interacted in an opposite orientation. (3) The multiple electrostatic interaction between the "soft nanoparticle" and SP1 is necessary. Computer simulations show that the generation 5 PAMAM dendrimer (PD5), with 128 terminal amino groups around the surface, is an optimal "soft nanoparticle" with a diameter of 5.3 nm (Scheme 1b).[20] The PD5 was synthesized according to the previously reported work and each step was characterized by ^{1}H NMR (see Supporting Information, Figures S1−S8).[18] We anticipate that this giant "soft nanoparticle" can set on the center of SP1 and be stabilized by surface−surface multiple electrostatic interactions between SP1 and PD5, and the exposed PD5 surface can interact with another SP1 to form a sandwiched structure, further assembling to ordered protein nanowires (Scheme 1d).

For assembling of SP1 into nanowire that would bury its top and bottom surfaces within the nanowire (except the two terminal rings), the catalytic site must be designed in the outer surface to avoid being shielded by PD5 nanoparticle. Computer simulations indicate that Ala 57 of SP1 is an ideal position for site-directed mutagenesis to design a GPx catalytic site; selenocysteine (Sec), for the catalytic center is located in a shallow pocket of SP1 outside surface and the substrate GSH can be stabilized by two arginine residues (Arg 16, Arg 61) (Scheme 2a). Se-SP1-57Cys was produced with the aid of cysteine auxotrophic expression system, and further characterized by MALDI-TOF mass spectrometry and CD spectra (see Supporting Information, Figures S9 and S10).

In addition, SOD catalytic centers, manganese porphyrin (MnPP), were synthesized and characterized by ^{1}H NMR and mass spectrometry (see Supporting Information, Figures S11−S13). The artificial SOD mimic (MnPD5) was prepared by Michael addition reaction between amino groups of PD5 and acrylic groups of MnPP. (Scheme 2b, see Supporting Information, Figure S14). UV−vis spectra indicated that there were 4.1 MnPP per MnPD5 macromolecule.

SP1 Based Assembly Induced by "Soft Nanoparticles". Dynamic light scattering (DLS) was used to investigate the size distribution of SP1−PD5 assembly (see Supporting Information, Figure S15). SP1 only scattered a uniform peak and the average hydrodynamic diameter (D_h) was close to its crystal size (11 nm), while a unimodal distribution with increasing D_h was observed with the addition of PD5, demonstrating that SP1 could interact with PD5 to form larger aggregates. The D_h of SP1−PD5 increased to 220 nm with the addition of 1.0 equiv PD5. To demonstrate the stability of the electrostatic structures, we further investigated the effect of ionic strengths, pH values, temperatures, and buffers on electrostatic assembly behaviors (see Supporting

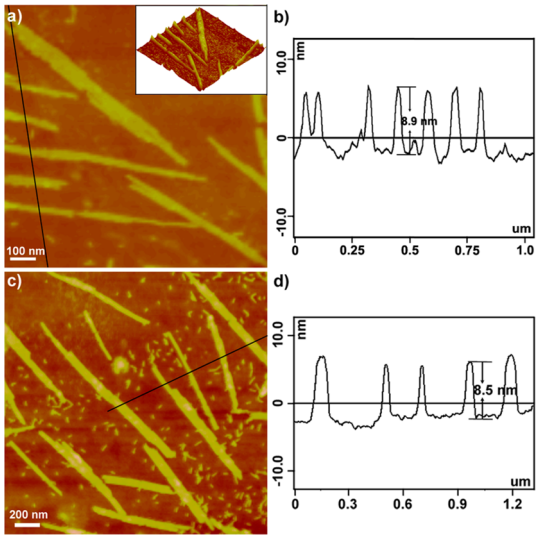

Figure 1. AFM images of cricoid SP1-based self-assembly induced by "soft nanoparticles" at the molar ratio of 1:1. (a) AFM topographical image of SP1−PD5 nanowires. Inset is the 3D image of (a). (b) Height profile along the black line in (a). (e) AFM image of SeSP1−MnPD5 nanowires. (f) Height profile along the black line in (e). The final concentration of SP1 or SeSP1 is 1.0 μM.

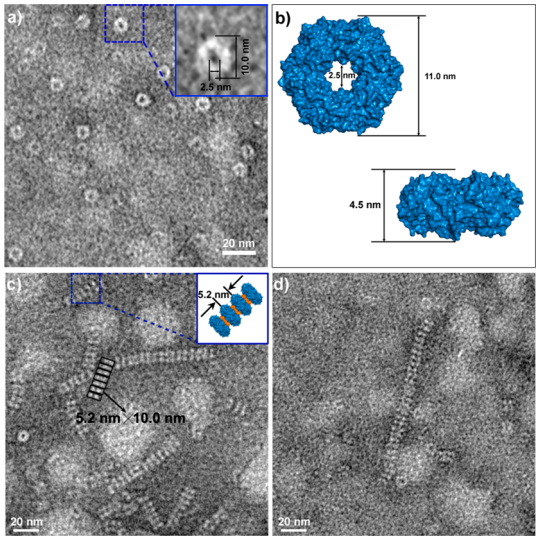

Figure 2. TEM images of cricoid SP1-based self-assembly induced by "soft nanoparticles". (a) TEM topographical image of pure SP1 nanorings. Inset is an amplified TEM image of the square. The sizes are calculated from TEM image. (b) Top and side views of theoretical pictures. The sizes are theoretical values. (c) TEM image of SP1−PD5 nanowires at the molar ratio of 1:1. Inset is the model of SP1−PD5 nanowire stacked with four SP1 ring and three PD5. (d) TEM image of SeSP1−MnPD5 nanowires.

Information, Figure S16). The nanowire structures were stable at low NaCl concentration (100 mM) or middle pH values (6−9). But they disassembled at higher NaCl concentration (400 mM) or at higher or lower pH values (2 or 12). We also found the temperature (4, 25, and 37 °C) or buffer (PBS, HEPES, and Tris-HCl) afforded limited impact on the assembly structures. The tapping-mode atomic force microscopy (AFM) images also showed that the morphologies of SP1−PD5 changed from nanospheres to nanowires when the PD5 increased from 0 equiv to 1.0 equiv (see Supporting Information, Figure S17). SP1 self-assembly induced by PD5 with the molar ratio of 1:1 could form ordered nanowires. The AFM images showed that SP1−PD5 could self-assemble to more than 100 nm in length. The uniform height (7.2 nm) was lower than the diameter of its crystal structure (approximately 11 nm), which was probably due to the skew arrangement of SP1 caused by soft PD5. Unlike those "rigid nanoparticles", PD5 was a multicavity molecule and difficult to support SP1 nanoring arranged vertically.

Figure 1a showed two SP1−PD5 nanowires could further be arranged in staggered gear-like arrays at higher concentration. We thought the exposed amino groups of PD5 nanoparticles could electrostatic interact with negative charges (for example Glu and Asp) around the SP1 outside surface of another nanowire.[17] Interestingly, the electrostatic interaction and the spatial complement could more effectively support SP1 nanoring standing upright. The height of the staggered nanowires was 8.9 nm, larger than that of single nanowire (Figure 1b). We further staked bundles of nanowires for clear observation (see Supporting Information, Figure S18b). As shown in Figure 1c,d, SeSP1 could also spontaneously assemble into nanowires with the addition of MnPD5, and the length of SeSP1−MnPD5 nanowires could reach 1 μm. Also, the height of the nanowires were measured to be 8.5 nm, in accordance with the SP1 assembly induced by PD5. All these AFM dates indicated that the introduction of GPx and SOD catalytic centers did not change the assembly morphologies obviously.

Transmission electron microscope (TEM) images further confirmed our hypothesis of the assembly mechanism. TEM image showed SP1 could get together by hydrophobic interactions to form cricoid proteins with the diameter of 10 nm, in accordance with its double-layered crystal structure (Figure 2a,b). Figure 2c showed the representative TEM image of SP1−PD5 nanowires and illustrated the predominant topological arrangement: extended, roughly linear structures composed of regular repeating SP1 units. The averaged image showed the repeating unit had an hourglass shape with dimensions of 5.2 nm × 10.0 nm, oriented perpendicularly to the C_6 symmetry axis of SP1. The ring−ring average distance (5.2 nm) was larger than the crystal width of single SP1 ring (4.5 nm), indicating that PD5 could serve as a linker to link two SP1 to form SP1−PD5 chains. To gain greater structural insight into the observed aggregates, we staked SP1−PD5 nanowire model composed of four repeating units (Figure 2c, inset). Figure 2d displayed one SeSP1−MnPD5 nanowire. Notably, the resulting morphology of the nanowire was full in accord with that of SP1−PD5 nanowires. All these data demonstrated these "soft nanoparticles"

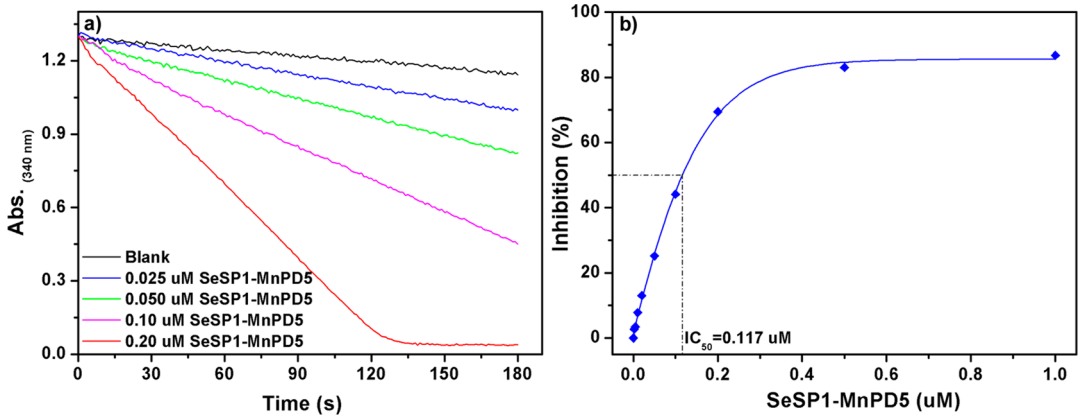

Figure 3. GPx and SOD activities of SeSP1−MnPD5 assemblies. (a) Plots of absorbance *versus* time during the catalytic reduction of H_2O_2 (0.5 mM) by GSH (1.0 mM) with 0 μM (black), 0.025 μM (blue), 0.050 μM (green), 0.10 μM (magenta), and 0.20 μM (red) SeSP1−MnPD5 at pH = 7.0 and 37 °C. (b) Percentage of inhibition of NBT oxidation by superoxide anion radical *versus* different concentrations of SeSP1−MnPD5.

TABLE 1. SOD and GPx Activities of SeSP1−MnPD5 and Other Mimics[a]

	GPx activity (μM·min^{-1}·μM^{-1})		SOD activity IC_{50} (μM)	
samples	one unit	assembly	one unit	assembly
SP1−PD5	~ 0	~ 0	~ 0	~ 0
SeSP1−MnPD5[b]	410 ± 20	(1.72 ± 0.08) × 10^4	0.117 ± 0.003	(2.79 ± 0.07) × 10^{-3}
Se-TMVcp142Cys[c]	185.9 ± 0.41	6320 ± 13.5	n.d.	n.d.
Ebselen[c]	1.02	1.02	n.d.	n.d.
GPx (rabbit liver)[c]	1445	5780	n.d.	n.d.
Cu−Zn SOD[d]	n.d.[e]	n.d.	1.3 × 10^{-3}	1.3 × 10^{-3}

[a] The measurements of GPx or SOD activities are showed in experimental method. [b] The GPx or SOD activities of one unit are showed as the catalytic rates per SeSP1 nanoring or per MnPD5 (containing 4.1 MnPP). Those of assembly are shown as the average catalytic rates for a nanowire. [c] Activity values are based on the ref 26. [d] Activity values are based on the ref 25. [e] n.d. refers to no detection.

(PD5, MnPD5) successfully interacted with cricoid proteins (SP1, SeSP1) along its C_6 symmetry axis by multiple surface−surface electrostatic interactions to form nanowires, which was exactly consistent with our previous expectations (Scheme 1d).

The GPx and SOD Activities of SeSP1−MnPD5. The GPx and SOD activities were evaluated as previously reported methods.[25−27] SP1−PD5 did not exhibit any antioxidative activities, while SeSP1−MnPD5 exhibited both excellent GPx and SOD activities (Figure 3, Table 1). The GPx activity was found to be 410 ± 20 μM·min^{-1}·μM^{-1} per SeSP1−MnPD5, which was comparable with the human plasma GPx and 400-fold higher than the commercially used Ebselen.[8] Also, The SOD activity of SeSP1−MnPD5 showed a measured IC_{50} of 0.117 ± 0.003 μM. For the SeSP1−MnPD5 nanowire, the average length was 220 nm. In other words, the SeSP1−MnPD5 nanowire was constructed by approximate 42 SeSP1 nanorings and 42 MnPD5 dendrimers (5.2 nm for a SeSP1−MnPD5). The SeSP1−MnPD5 nanowires showed significantly high GPx activity ((1.72 ± 0.08) × 10^4 μM·min^{-1}·μM^{-1}) and SOD activity ((2.79 ± 0.07) × 10^{-3} μM), approaching that of native rabbit liver GPx and Cu−Zn SOD.[25,26] DLS and AFM were further applied to investigate the structure stability (see Supporting Information, Figure S19). We found the size was nearly unchanged, and nanowire structures were still present after the catalytic reactions. Therefore, the nanowires not only afforded excellent GPx and SOD activities, but also processed perfect stability.

Michaelis−Menten model was also applied to investigate the dependency of SeSP1−MnPD5 enzymatic kinetic rate on the substrate concentration for the reduction of H_2O_2 by GSH (see Supporting Information, Figure S20). The data in the Table 2 were calculated from the plots in Supporting Information Figure S20 with the following equation:

$$\frac{\vartheta_0}{[E_0]} = \frac{k_{cat}[GSH][H_2O_2]}{K_{GSH}[H_2O_2] + K_{H_2O_2}[GSH] + [GSH][H_2O_2]}$$

The apparent Michaelis constant (K_{GSH}) and the first-order constant (k_{cat}) of SeSP1−MnPD5 at 1.0 mM GSH were measured to be 0.148 ± 0.006 mM and 460 ± 40 min^{-1}, respectively. The apparent second-order rate constant (k_{cat}/K_{GSH}) was (2.8 ± 0.2) × 10^6 M^{-1}·min^{-1}, only 1 order of magnitude less than that of natural GPx (2.7 × 10^7 M^{-1}·min^{-1}),[26,28] which was attributed to the effective GSH binding pockets forming at the outside of

the SP1 ring as previously designed. Also, the apparent second-order rate constant (k_{cat}/K_{H2O2}) of SeSP1−MnPD5 at 0.50 mM H_2O_2 was (9.8 ± 0.9) × 10^5 $M^{-1}\cdot min^{-1}$.

Antioxidative Capacity of SeSP1−MnPD5. SeSP1−MnPD5 could not only catalyze the reduction of H_2O_2 by GSH, but also scavenge the $O_2^{-\bullet}$ effectively. To evaluate the cooperative antioxidative capacity of SeSP1−MnPD5, we performed an assay of mitochondria oxidative stress. Once having suffered from the damage of the oxidative stress, the mitochondria would swell, resulting in the decrease of the absorption. The swelling level of mitochondria (SLM) was measured by monitoring the absorbance at 520 nm (Figure 4a).[26] Absorption of the mitochondria was dramatically decreased when it was incubated with sulfate/ascorbate. When 0.10 μM of antioxidative enzyme mimics were added to the system, the decrease degree of mitochondria absorption reduced. On the other hand, the production of the final oxidative product in a lipid peroxidation reaction, malondialdehyde (MDA), was further applied by using the thiobarbituric acid (TBA) assay. Inhibition of MDA content was determined as the absorbance at 532 nm. As shown in Figure 4b, MDA content decreased with the addition of enzyme mimics. The dual-enzyme cooperative antioxidative nanowires are far better than the uncooperative enzymes. Specifically, the absorption dropped from 0.128 to 0.065 after adding 0.10 μM SeSP1−MnPD5 for 50 min, with the inhibition ratio of nearly 60%, while the largest ratio is only 45% for the uncooperative enzymes (SP1−MnPD5 and SeSP1−PD5) (Figure 4c). SP1−MnPD5 or SeSP1−PD5 partly inhibited the MDA content, for they could only remove $O_2^{-\bullet}$ or H_2O_2. Also, the decrement of SLM reduced from 0.384 to 0.174 after 20 min for SeSP1−MnPD5, but they could only reduce to 0.339 and 0.253 for SP1−MnPD5 and SeSP1−PD5, respectively (Figure 4d). All these results suggested that the cooperation of GPx and SOD mimics could more effectively scavenged H_2O_2 and $O_2^{-\bullet}$ in the system and protect organisms from being damaged.

TABLE 2. Apparent Kinetic Parameters for H_2O_2 Reduction by GSH Catalyzed by SeSP1−MnPD5 Nanowires (SeSP1−MnPD5 as Catalytic Unit)

GSH (mM)	K_{cat} ($\times 10^2$ min^{-1})	K_{GSH} (mM)	K_{cat}/K_{GSH} ($\times 10^6$ M^{-1} min^{-1})
1.0	4.6 ± 0.4	0.148 ± 0.006	2.8 ± 0.2
H_2O_2 (mM)	**K_{cat} ($\times 10^2$ min^{-1})**	**K_{H2O2} (mM)**	**K_{cat}/K_{H2O2} ($\times 10^6$ M^{-1} min^{-1})**
0.50	5.6 ± 0.3	0.57 ± 0.02	0.98 ± 0.09

The cellular uptake behavior and the *in vitro* cytotoxicity of the nanowires toward human lung A549 cell line were investigated to disclose the biological effects.[29,30] The cellular nuclei were stained with 4′,6-diamidino-2-phenylindole (DAPI, blue), and fluorescein

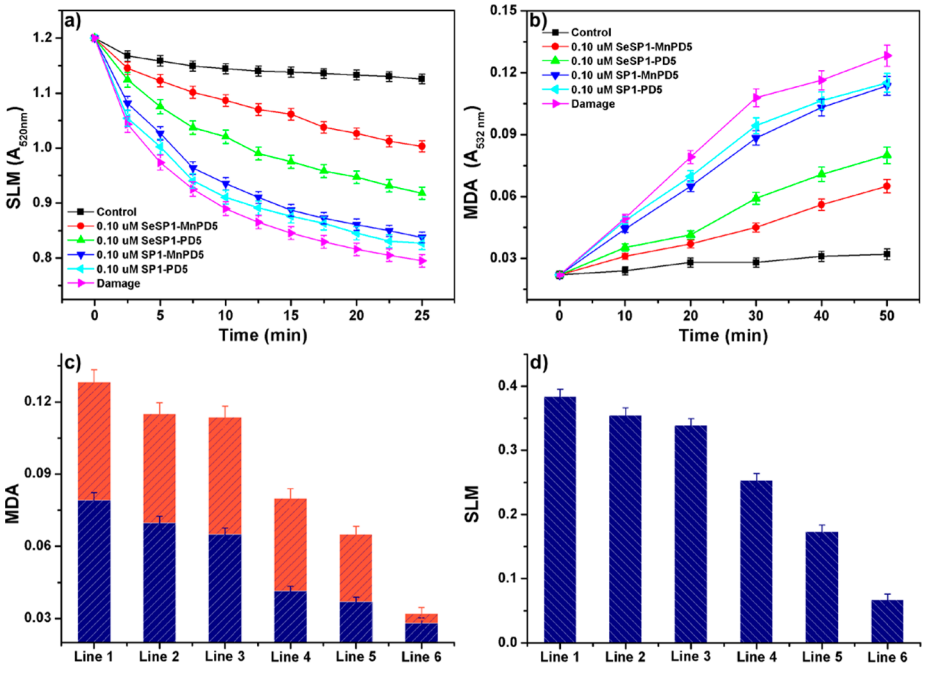

Figure 4. Plots of the inhibition of mitochondria damage to the swelling level of mitochondria (SLM) (a) and the level of lipid peroxidation (MDA) (b) with SeSP1−MnPD5 (red), SeSP1−PD5 (green), SP1−MnPD5 (blue), SP1−PD5 (cyan) or without ascorbate, ferrous and enzyme mimic (magenta). The black line is control test. (c) Inhibition of MDA content within 20 min (blue) and 50 min (blue+orange) under different antioxidative enzyme mimics. (d) Change of SLM within 20 min under different antioxidative enzyme mimics. Line 1 is damage test without enzyme mimic. Lines 2, 3, 4, and 5 are damage tests with 0.10 μM of SP1−PD5, SP1-MnSP1, SeSP1−PD5 and SeSP1−MnPD5, respectively. Line 6 is the control without ascorbate, ferrous and enzyme mimic.

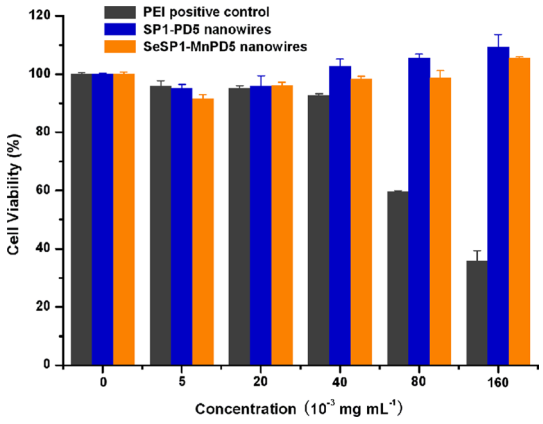

Figure 5. *In vitro* cytotoxicity assays of PEI-25K positive control (gray), SP1−PD5 nanowires (blue) and SeSP1−MnPD5 nanowires (orange) in different concentrations toward human lung A549 cell line.

isothiocyanate (FITC, green)-labeling-SP1 or FITC-labeling-PD5 of the nanowires were developed for subcellular observation, respectively. Confocal laser scanning microscopy (CLSM) images (see Supporting Information, Figure S21) showed no matter labeling SP1 or PD5 of the nanowires; the green fluorescence was observed in the cells and distributed widely in the cytoplasm after incubation for 3 h, suggesting that the nanowires could be successfully internalized by tumor cells *via* endocytosis. The *in vitro* cytotoxicity of the nanowires was evaluated by MTT assay, using PEI-25K as the positive control (Figure 5). The relative cell viability (RSV) was calculated as

$$\mathrm{RSV}(\%) = \frac{A_{\mathrm{Sample}}}{A_0} \times 100\ (\%)$$

where A_{sample} and A_0 were denoted as the absorbance values of the sample with and without enzyme mimic, respectively. After 24 h of incubation, SP1−PD5 exhibited almost no cytotoxicity to the cells even at concentrations as high as 0.16 mg·mL^{-1}, indicating that our enzymatic scaffold has low cytotoxicity and good biocompatibility. After introducing Sec and MnPP, the SeSP1−MnPD5 also processed ultralow cytotoxicity and excellent biocompatibility, while nearly 65% of cells died with the addition of 0.16 mg·mL^{-1} of PEI-25K.

CONCLUSIONS

In conclusion, we developed a novel strategy to construct high-ordered protein nanowires by "soft nanoparticles" induced self-assembly of cricoid proteins. Multiple electrostatic interactions between electropositive "soft nanoparticles" and electronegative cricoid proteins were employed to control the protein self-assembly behavior. Atomic force microscopy and transmission electron microscopy showed one "soft nanoparticle" (PD5) could electrostatically interact with two cricoid proteins (stable protein one, SP1) in an opposite orientation to form sandwich structure, further leading to self-assembled protein nanowires. Also, two nanowires could further be arranged in staggered gear-like arrays at high concentration. We further designed a dual-enzyme cooperative antioxidative system (SeSP1−MnPD5) with both GPx and SOD activities by means of inducing catalytic Sec and MnPP to SP1 and PD5, respectively. The multienzyme-functionalized protein nanowires showed significant biological effect over that of single enzyme in protecting mitochondria against oxidative stress and had low cytotoxicity and good biocompatibility with human cells. We anticipate this novel strategy should become a promising way to develop multifunctional bionanomaterials for catalysis, biosensors or pharmaceuticals.

EXPERIMENTAL SECTION

Synthesis of "Soft Nanoparticles" (PD5, MnPD5). The synthesis procedure of PD5 was shown in the Supporting Information (Figures S1−S8). 1, 2-Ethylenediamine was employed as core and reacted with methyl acrylate by Michael addition reaction to form quaternary ester. Then, the quaternary ester was aminated with excess 1,2-ethylenediamine to form quaternary amide, as generation zero (PAMAM G0). We could get different generation PAMAM dendrimer by alternatively Michael additions and amination reactions.

MnPD5 was prepared by Michael addition reaction between amino groups of PD5 and acrylic groups of MnPP (see Supporting Information, Figures S11−S14). The MnPP content of MnPD5 was determined by UV−vis spectra. Specifically, MnPP was dissolved in methanol at different concentrations (0.005, 0.01, 0.02, and 0.03 mM) and the absorption values were determined at 463 nm. The absorption value of MnPP *vs* concentration to plot and getting the regression equation: $y = 19.0x + 0.034$. The absorption value of MnPD5 at 3.80 μM was determined to be 0.330, so there were 4.1 MnPP molecules per MnPD5 ($n = 4.1$).

Construction of Catalytic Centers on SP1. The construction of plasmids containing SP1 genes encoding were carried out as our previously reported method.[15] Site-directed PCR was carried out by using the primers PU1 (5′-GGCATGGAGTCTTGTGAGCTAAACC-3′) and PD1 (5′-CTCGGTTTAGCTCACAAGACTCCAT-3′) to remove cysteine codon at site 57, and the recombined plasmid pET-SP1-22b was confirmed by DNA sequencing (Sangon). The Se-SP1-57Cys was expressed by transformed pET-SP1-22b plasmids into *Escherichia coli* BL21 and grew in 1 L M9 expression medium containing cysteine hydrochloride (50 pg·mL^{-1}) with shaking at 37 °C. After OD600 reaching to 1.0, protein expression was expressed for 30 min by addition of IPTG (1.0 mM), and then chloramphenicol (10 pg·mL^{-1}) was mixed into the culture for another 10 min. Then, the cleaned cells were suspended in the M9 production medium containing DL-selenocysteine (100 pg·mL^{-1}). The cells were collected after induction at 28 °C for 3 h. After cell ultrasonication and centrifugation, the mixture was heated at 85 °C for 20 min and further purified by DEAE column and dialyzed with an 8 kDa cut off dialysis membrane to milli-Q water and stored at −20 °C. Se-SP1-57Cys was further characterized by MALDI-TOF MS and CD spectra (see Supporting Information, Figures S9 and S10).

SP1-Based Self-Assembly Induced by "Soft Nanoparticles". The assembly of SP1−PD5 nanowires was as follow: SP1 or PD5 was

dissolved in Milli-Q with the concentration of 2.0 μM. Then, 100 μL of PD5 was mixed with 100 μL of SP1 solution at 4 °C. The mixed solutions were ultrasonicated for 10 min and then let stand for 30 min before use. The assembly of SeSP1−MnPD5 nanowires was similar to the assembly of SP1−PD5 nanowires.

GPx and SOD Analysis of SeSP1−MnPD5. The GPx activity was measured by a coupled reductase method as described previously.[24] The reaction was carried out at 37 °C in 500 μL of solution containing 50 mM potassium phosphate buffer (pH = 7.0, 1.0 mM EDTA), 1.0 mM GSH, 1.0 U of glutathione disulfide (GSSG) reductase, and appropriate GPx mimic. The mixture was incubated at 37 °C for 3 min, and then 0.50 mM H_2O_2 was added to initiate reaction. The activity was determined by measuring the absorbance decrease of NADPH at 340 nm (ε = 6220 $M^{-1}\cdot cm^{-1}$, pH = 7.0) using SHIMADZU UV-2450 UV/vis spectrophotometer. The activity unit was defined as the amount of the enzyme mimic that catalyzed the turnover of 1 μmol of NADPH per minute and described as $\mu mol\cdot min^{-1}\cdot \mu mol^{-1}$.

The SOD activity was determined using the standard xanthine/xanthine oxidase (XOD) assay system developed by McCord and Fridovich.[27] Superoxide radical anions ($O_2^{-\bullet}$) were generated by the xanthine/XOD system at 37 °C (50 mM phosphate buffer containing 0.1 mM EDTA, pH = 7.8). XOD (0.025 $U\cdot mL^{-1}$) was added to 50 mM phosphate buffer containing 0.3 mM xanthine, 0.1 mM NBT, and appropriate amounts of enzyme to monitor the oxidation of NBT to blue formazane (MF^+) at 560 nm using SHIMADZU UV-2450 UV/vis spectrophotometer. The enzyme concentration with a 50% inhibition of the rate of oxidation of nitrotetrazolium blue chloride (NBT) (IC_{50}) was used to evaluate the SOD activity.

Bioantioxidant Capacity of SeSP1−MnPD5. The swelling level of mitochondria (SLM) was carried out with the absorption at 520 nm by UV absorption according to our previously reported methods. Specifically, bovine heart mitochondria were extracted from fresh bovine heart. To a mixture solution containing 25 mM HEPES-NaOH buffer (pH = 7.4, 0.3 mM EDTA), KCl (0.125 M), $MgCl_2$ (1.0 mM), mitochondria (0.5 $mg\cdot mL^{-1}$), GSH (1.0 M) and 0.10 μM of antioxidative enzyme mimic were added ascorbate (0.5 mM) and ferrous sulfate (12.5 μM) at 37 °C. The turbidity degree was measured by monitoring the 520 nm absorption at different time. The control experiment was performed without enzyme mimic, ascorbate and ferrous sulfate. The SLM was used as the absorption of the sample to evaluate the antioxidative effect. Data was presented as average ± SD (n = 3).

The level of lipid peroxidation was determined by measuring the absorption of the reaction product between thiobarbituric acid (TBA) and the final product of lipid peroxidation malondialdehyde (MDA) at 532 nm ($\varepsilon = 1.56 \times 10^5\ M^{-1}\cdot cm^{-1}$). The procedure was as follows: 1 mL of trichloroacetic acid (70 $g\cdot L^{-1}$) and 1 mL of TBA (5.0 $g\cdot L^{-1}$) were added into 1 mL of above mixture at 80 °C for certain time. When cooled to room temperature, the mixture was centrifuged at 3000 rpm for 10 min and the supernatant was used to measure the absorption at 532 nm. The control experiment was performed without enzyme mimic, ascorbate and ferrous sulfate. Data was presented as average ± SD (n = 3).

Cellular Uptake Behavior. The cellular uptake behavior of the florescence labeled nanowires was investigated by confocal laser scanning microscopy (CLSM) toward A549 cells.[30] FITC-labeled (green) nanowires were developed for subcellular observation. The cells were seeded on coverslips in 6-well plates in 2 mL of Dulbecco's modified Eagle's medium (DMEM) and cultured for 3 h at 37 °C. The original medium was replaced with FITC-labeling SP1 or FITC-labeling PD5 of the nanowires. The cells were fixed with 4% formaldehyde for 20 min at room temperature after 3 h incubation. The cell nuclei were stained by DAPI according to the standard protocol provided by the supplier.

Cell Cytotoxicity. A human cancer line, lung carcinoma (A549), was cultured in DMEM with high glucose containing 10% fetal bovine serum (FBS), supplemented with 50 $U\cdot mL^{-1}$ penicillin and 50 $U\cdot mL^{-1}$ streptomycin, and was seeded in 96-well plates to 7000 cells per well in 0.1 mM DMEM medium and incubated at 37 °C in 5% CO_2 atmosphere for 24 h.[29,30] After removing culture medium, the SP1−PD5 or SeSP1−MnPD5 at different concentrations (0−0.16 $mg\cdot mL^{-1}$) was added and the cells were subjected to thiazolyl blue tetrazolium bromide assay after being incubated for another 24 h. PEI-25K was used as positive control to evaluate the sample cytotoxicity. The absorbance of the solution was measured as the cell concentration on a Bio-Rad 680 microplate reader at 492 nm. Data was presented as average ± SD (n = 3).

Conflict of Interest: The authors declare no competing financial interest.

Supporting Information Available: The detail synthesis procedures and characterization (^{1}H NMR or ESI) of PD5 and MnPD5; MALDI-TOF mass spectrometry and CD spectra of SeSP1; electrostatic assembly behaviors of the SP1−PD5 aggregates; electrostatic stability investigation of SP1−PD5 aggregates; SP1−PD5 aggregates morphologies with various ratios of PD5; stability investigation of SeSP1−MnPD5 aggregates after catalytic reactions; enzymatic activity determination and the cellular uptake behavior of the SeSP1−MnPD5 aggregates. The Supporting Information is available free of charge on the ACS Publications website at DOI: 10.1021/acsnano.5b01311.

Acknowledgment. We thank Oded Shoseyov from the Hebrew University of Jerusalem for his kind supply of the SP1 gene. This work was supported by the Natural Science Foundation of China (No: 21234004, 21420102007, 21221063, 21474038), 111 project (B06009) and the Chang Jiang Scholars Program of China.

REFERENCES AND NOTES

1. Yan, H.; Park, S. H.; Finkelstein, G.; Reif, J. H.; LaBean, T. H. DNA-Templated Self-Assembly of Protein Arrays and Highly Conductive Nanowires. *Science* **2003**, *301*, 1882–1884.
2. Niu, Z. W.; Liu, J.; Lee, L. A.; Bruckman, M. A.; Zhao, D. G.; Koley, G.; Wang, Q. Biological Templated Synthesis of Water-Soluble Conductive Polymeric Nanowires. *Nano Lett.* **2007**, *7*, 3729–3733.
3. Ballister, E. R.; Lai, A. H.; Zuckerman, R. N.; Cheng, Y. F.; Mougous, J. D. *In Vitro* Self-Assembly from a Simple Protein of Tailorable Nanotubes Building Block. *Proc. Natl. Acad. Sci. U.S.A.* **2008**, *105*, 3733–3738.
4. Reuel, N. F.; Grassbaugh, B.; Kruss, S.; Mundy, J. Z.; Opel, C.; Egodage, K.; Wahl, R.; Helk, B.; Zhang, J. Q.; Strano, M. S.; et al. Emergent Properties of Nanosensor Arrays: Applications for Minitoring IgG Affinity Distributions, Weakly Affined Hypermannosylation, and Colony Selection for Biomanufacturing. *ACS Nano* **2013**, *7*, 7472–7482.
5. Huang, X.; Li, M.; Green, D. C.; Williams, D. S.; Patil, A. J.; Mann, S. Interfacial Assembly of Protein-Polymer Nanoconjugates into Stimulus-Responsive Biomimetic Protocells. *Nat. Commun.* **2013**, *4*, 2239–2247.
6. Keskin, O.; Gursoy, A.; Ma, B.; Nussinov, R. Principles of Protein-Protein Interactions: What Are the Preferred Ways for Proteins to Interact? *Chem. Rev.* **2008**, *108*, 1225–1244.
7. Chen, C. L.; Bromley, K. M.; Moradian-Oldak, J.; DeYoreo, J. J. *In Situ* AFM Study of Amelogenin Assembly and Disassembly Dynamics on Charged Surfaces Provides Insights on Matrix Protein Self-Assembly. *J. Am. Chem. Soc.* **2011**, *133*, 17406–17413.
8. Hou, C. X.; Li, J. X.; Zhao, L. L.; Zhang, W.; Luo, Q.; Dong, Z. Y.; Xu, J. Y.; Liu, J. Q. Construction of Protein Nanowires through Cucurbit[8]uril-based Highly Specific Host−Guest Interactions: An Approach to the Assembly of Functional Proteins. *Angew. Chem., Int. Ed.* **2013**, *52*, 5590–5593.
9. Biswas, S.; Kinbara, K.; Niwa, T.; Taguchi, H.; Ishii, N.; Watanabe, S.; Miyata, K.; Kataoka, K.; Aida, T. Biomolecular Robotics for Chemomechanically Driven Guest Delivery Fuelled by Intracellular ATP. *Nat. Chem.* **2013**, *5*, 613–620.
10. Li, T.; Zan, X. J.; Winans, R. E.; Wang, Q.; Lee, B. Biomolecular Assembly of Thermoresponsive Superlattices of the Tobacco Mosaic Virus with Large Tunable Interparticle Distances. *Angew. Chem., Int. Ed.* **2013**, *52*, 6638–6642.

11. Boerakker, M. J.; Hannink, J. M.; Bomans, P. H. H.; Frederik, P. M.; Nolte, R. J. M.; Meijer, E. M.; Sommerdijk, N. A. J. M. Giant Amphiphiles by Cofactor Reconstitution. *Angew. Chem., Int. Ed.* **2002**, *41*, 4239–4241.
12. Ghosh, P. S.; Kim, C. K.; Han, G.; Forbes, N. S.; Rotello, V. M. Efficient Gene Delivery Vectors by Tuning the Surface Charge Density of Amino Acid-Functionalized Gold Nanoparticles. *ACS Nano* **2008**, *2*, 2213–2218.
13. Wang, W. X.; Pelah, D.; Alergand, T.; Shoseyov, O.; Altam, A. Characterization of SP1, a Stress-Responsive, Boiling-Soluble, Homo-Oligomeric Protein from Aspen. *Plant Physiol.* **2002**, *130*, 865–875.
14. Dgany, O.; Gonzalez, A.; Sofer, O.; Wang, W. X.; Zolotnitsky, G.; Wolf, A.; Shoham, Y.; Altman, A.; Wolf, S. G.; Shoseyov, O.; Almog, O. The Structural Basis of the Thermostability of SP1, a Novel Plant (Populus tremula) Boiling Stable Protein. *J. Biol. Chem.* **2004**, *279*, 51516–51523.
15. Miao, L.; Zhang, X. Y.; Si, C. Y.; Gao, Y. Z.; Zhao, L. L.; Hou, C. X.; Shoseyov, O.; Luo, Q.; Liu, J. Q. Construction of a Highly Stable Artificial Glutathione Peroxidase on a Protein Nanoring. *Org. Biomol. Chem.* **2014**, *12*, 362–369.
16. Medalsy, I.; Dgany, O.; Sowwan, M.; Cohen, H.; Yukashevska, A.; Wolf, S. G.; Wolf, A.; Koster, A.; Almog, O.; Marton, I.; et al. SP1 Protein-Based Nanostructures and Arrays. *Nano Lett.* **2008**, *8*, 473–477.
17. Miao, L.; Han, J. S.; Zhang, H.; Zhao, L. L.; Si, C. Y.; Zhang, X. Y.; Hou, C. X.; Luo, Q.; Xu, J. Y.; Liu, J. Q. Quantum-Dot-Induced Self-Assembly of Cricoid Protein for Light Harvesting. *ACS Nano* **2014**, *8*, 3743–3751.
18. Tomalia, D. A.; Baker, H.; Dewald, J.; Hall, M.; Kallos, G.; Martin, S.; Roeck, J.; Ryder, J.; Smith, P. A New Class of Polymers: Starburst-Dendritic Macromolecules. *Polym. J.* **1985**, *17*, 117–132.
19. Tomalia, D. A.; Naylor, A. M.; Goddard, W. A., III Starburst Dendrimers: Molecular-Level Control of Size, Shape, Surface Chemistry, Topology, and Flexibility from Atoms to Macroscopic Matter. *Angew. Chem., Int. Ed. Engl.* **1990**, *29*, 138–175.
20. Esfand, R.; Tomalia, D. A. Poly (amidoamine) (PAMAM) Dendrimers: From Biomimicry to Drug Delivery and Biomedical Applications. *Drug Discovery Today* **2001**, *6*, 427–436.
21. Huang, X.; Liu, X. M.; Luo, Q.; Liu, J. Q.; Shen, J. C. Artificial Selenoenzymes: Designed and Redesigned. *Chem. Soc. Rev.* **2011**, *40*, 1171–1184.
22. Dong, Z. Y.; Luo, Q.; Liu, J. Q. Artificial Enzymes Based on Supramolecular Scaffolds. *Chem. Soc. Rev.* **2012**, *41*, 7890–7908.
23. Lin, Y. H.; Ren, J. S.; Qu, X. G. Nano-Gold as Artificial Enzymes: Hidden Talents. *Adv. Mater.* **2014**, *26*, 4200–4217.
24. Oshikawa, K.; Shi, F. S.; Rakhmilevich, A. L.; Sondel, P. M.; Mahvi, D. M.; Yang, N. S. Synergistic Inhibition of Tumor Growth in a Murine Mammary Adenocarcinoma Model by Combinational Gene Therapy using IL-12, pro-IL-18, and IL-1 beta Converting Enzyme cDNA. *Proc. Natl. Acad. Sci. U.S.A.* **1999**, *96*, 13351–13356.
25. Gao, Y. Z.; Hou, C. X.; Zhou, L. P.; Zhang, D. M.; Zhang, C. Q.; Miao, L.; Wang, L.; Dong, Z. Y.; Luo, Q.; Liu, J. Q. A Dual Enzyme Microgel with High Antioxidant Ability Based on Engineered Seleno-Ferritin and Artificial Superoxide Dismutase. *Macromol. Biosci.* **2013**, *13*, 808–816.
26. Hou, C. X.; Luo, Q.; Liu, J. L.; Miao, L.; Zhang, C. Q.; Gao, Y. Z.; Zhang, X. Y.; Xu, J. Y.; Dong, Z. Y.; Liu, J. Q. Construction of GPx Active Centers on Natural Protein Nanodisk/Nanotube: A New Way to Develop Artificial Nanoenzyme. *ACS Nano* **2012**, *6*, 8692–8701.
27. McCord, J. M.; Fridovich, I. Superoxide Dismutase. An Enzymic Function for Erythrocuprein (Hemocuprein). *J. Biol. Chem.* **1969**, *244*, 6049–6055.
28. Maiorino, M.; Roche, C.; Kiess, M.; Koenig, K.; Gawlik, D.; Matthes, M.; Naldini, E.; Pierce, R.; Flohe, L. A Selenium-Containing Phospholipid-Hydroperoxide Glutathione Peroxidase in Schistosoma Mansoni. *Eur. J. Biochem.* **1996**, *238*, 838–844.
29. Zhang, Y.; Xiao, C. S.; Li, M. Q.; Ding, J. X.; He, C. L.; Zhuang, X. L.; Chen, X. S. Core-cross-linked Micellar Nanoparticles from a Linear-Dendritic Prodrug for Dual-Responsive Drug Delivery. *Polym. Chem.* **2014**, *5*, 2801–2808.
30. Lv, S. X.; Tang, Z. H.; Li, M. Q.; Lin, J.; Song, W. T.; Liu, H. Y.; Huang, Y. B.; Zhang, Y. Y.; Chen, X. S. Co-delivery of Doxorubicin and Paclitaxel by PEG-Polypeptide Nanovehicle for the Treatment of Non-small Cell Lung Cancer. *Biomaterials* **2014**, *35*, 6118–6129.